




Ultrahigh-resolution anterior segment optical coherence tomography for analysis of corneal microarchitecture during wound healing

Anca Pantalon,^{1,2}  Martin Pfister,^{1,3} Valentin Aranha dos Santos,¹ Sabina Sapeta,¹ Angelika Unterhuber,¹ Niklas Pircher,⁴ Gerald Schmidinger,⁴ Gerhard Garhöfer,⁵ Doreen Schmidl,⁵  Leopold Schmetterer^{1,3,6,7,8,9} and René M. Werkmeister^{1,3} 

¹Center for Medical Physics and Biomedical Engineering, Medical University of Vienna, Vienna, Austria

²Department of Ophthalmology, Gr. T. Popa University of Medicine and Pharmacy, Iasi, Romania

³Christian Doppler Laboratory for Ocular and Dermal Effects of Thiomers, Medical University of Vienna, Vienna, Austria

⁴Department of Ophthalmology, Medical University of Vienna, Vienna, Austria

⁵Department of Clinical Pharmacology, Medical University of Vienna, Vienna, Austria

⁶Singapore Eye Research Institute, Singapore National Eye Centre, Singapore, Singapore

⁷Ophthalmology and Visual Sciences Academic Clinical Program, Duke-NUS Medical School, Singapore, Singapore

⁸Ophthalmic Engineering & Innovation Laboratory, Department of Biomedical Engineering, Faculty of Engineering, National University of Singapore, Singapore, Singapore

⁹Lee Kong Chian School of Medicine, Nanyang Technological University, Singapore, Singapore

ABSTRACT.

Purpose: To employ ultrahigh-resolution (UHR) optical coherence tomography (OCT) for investigation of the early wound healing process in corneal epithelium.

Methods: A custom-built UHR-OCT system assessed epithelial healing in human keratoconic cornea after epi-off crosslinking (CXL) procedure and a wound healing model in rabbits with iatrogenic corneal injury. 3D OCT data sets enhanced obtaining epithelial thickness maps and evaluation of reepithelization stage. Accompanying changes in deeper corneal microarchitecture were analysed.

Results: The mean central corneal thickness in 40 eyes with keratoconus at baseline was $482.7 \pm 38.2 \mu\text{m}$, while mean central epithelial thickness (CET) was $43.8 \pm 6.4 \mu\text{m}$. At the final visit 20 ± 5 days post-CXL procedure, CET was $35.0 \pm 5.8 \mu\text{m}$, significantly thinner after reepithelization ($p < 0.001$). Surgical success was assessed at the final visit through the demarcation line (DL), identified at $43.7 \pm 13.5\%$ stromal depth. In rabbits, the mean CET in 20 eyes at baseline was $35.9 \pm 2.6 \mu\text{m}$. In rabbits that revealed complete wound closure (10/20 eyes) at the last study day at 72 hr, CET was significantly thinner compared to baseline ($30.4 \pm 2.8 \mu\text{m}$ versus $35.4 \pm 2.9 \mu\text{m}$, $p = 0.005$). An intra-stromal landmark indicating early keratocyte apoptosis was measured at $30.0 \pm 5.1\%$ stromal depth. Epithelial thickness maps showed the time-course of corneal healing.

Conclusion: Ultrahigh-resolution (UHR)-OCT provided precise assessment of epithelial wound and its healing by 3D-mapping. In addition, microarchitectural changes in the cornea in early phases of epithelial healing were revealed.

Key words: cornea – epithelium – optical coherence tomography – wound healing

Acta Ophthalmol. 2019; 97: e761–e771

© 2019 The Authors. Acta Ophthalmologica published by John Wiley & Sons Ltd on behalf of Acta Ophthalmologica Scandinavica Foundation.

This is an open access article under the terms of the Creative Commons Attribution-NonCommercial-NoDerivs License, which permits use and distribution in any medium, provided the original work is properly cited, the use is non-commercial and no modifications or adaptations are made.

doi: 10.1111/aos.14053

Introduction

The cornea is the main refractive element in human eyes and its integrity

influences vision both qualitatively and quantitatively (Liu & Kao 2015; Fischak et al. 2017). Changes in its microarchitecture are caused by a

variety of conditions: ectatic, traumatic, inflammatory or infectious (Werkmeister et al. 2017). When any type of corneal injury occurs, a healthy

cornea with enough regenerative capacity is capable to repair the structural defect and restore visual function. Yet, excluding minor superficial epithelial scratches, few corneal injuries heal completely with restoration of both structure and function (McGrath & Lee 2013). Most corneal healing processes implicate scar tissue formation, which has low tensile strengths and does not provide the same high optical quality as healthy cornea does (McGrath & Lee 2013). Epithelial, stromal and endothelial corneal wounds heal by various mechanisms (Ljubimov & Saghizadeh 2015), some being general, some being cell specific. The type of corneal injury and the extent of damage dictate the intensity of the wound healing response (McGrath & Lee 2013). During the corneal wound healing process, the dynamics of the epithelium (EP) are of utmost importance, since it is capable of modulating its thickness to restore corneal integrity, maintain smooth surface and provide optical symmetry of the cornea. Its 'compensatory' property for the changes in the layers beneath (e.g. stroma) is unique and critical for corneal healing. The most frequent example is given by the early stages of keratoconus, where the back stromal surface changes are easily identified by anterior segment optical coherence tomography (AS-OCT), while the front surface changes, if minor, can be completely masked by epithelial remodelling (Zhou & Stojanovic 2014). Several studies have demonstrated the important role of Bowman's layer (BL) in modulating stromal wound healing (Lagali et al. 2009; Luo et al. 2015; Shroff et al. 2016) and restoration of subepithelial nerve plexus (Lagali et al. 2009).

Until now, various methods have been used for assessing corneal structure starting from the conventional slit lamp biomicroscopy, towards more complex imaging technologies such as the AS-OCT (Grieve et al. 2004; Yasuno et al. 2005; Gora et al. 2009), ultrasound biomicroscopy (Reinstein et al. 2014), corneal epithelial 3D mapping by very high-frequency digital ultrasound (Reinstein et al. 2015) or confocal microscopy (Guthoff et al. 2009). Recently, important advancements have been achieved in the AS-OCT field, where ultrahigh-resolution (UHR) OCT enabled very accurate imaging of

all corneal layers, including precise assessment of the precorneal tear film (Schmoll et al. 2012; Werkmeister et al. 2013) and accurate extraction of tear film thickness maps (Aranha Dos Santos et al. 2015). Furthermore, based on the acquired three-dimensional data sets, epithelial thickness maps could be extracted and correlated with Scheimpflug tomography maps (Werkmeister et al. 2017). In the recent literature, epithelial thickness maps yielded by spectral-domain OCT data analysis have been described as useful imaging tools before and after crosslinking (CXL) interventions in keratoconus patients (Rocha et al. 2014; Zhou & Stojanovic 2014), giving evidence that an UHR imaging approach might provide an insight even into more subtle changes related to the intervention and the healing after. In addition, with its outstanding depth resolution in the range of 1.2 μm , the system provides an 'optical biopsy' in a rapid, non-invasive, non-contact manner revealing morphology of the probed tissues by detecting its different optical properties.

Aim of our study was to investigate the capability of a custom-built UHR-OCT system to assess the corneal wound healing process and to document the accompanying microarchitectural changes in two different conditions: a wound healing model in rabbits with iatrogenic corneal injury and human keratoconic cornea after epi-off CXL procedure.

Patients and Methods

Experimental paradigm

Patients with keratoconus

The present analysis included patients diagnosed with keratoconus from a study performed at the Department of Clinical Pharmacology and the Center of Medical Physics and Biomedical Engineering at the Medical University of Vienna. The study was performed in adherence to the Declaration of Helsinki (World Medical Association 2013) and to the Good Clinical Practice guidelines. The study protocol was approved by the Ethics Committee of the Medical University of Vienna (Vienna, Austria). Selection criteria, study design and surgical intervention [accelerated epi-off CXL, 10 min irradiation with UVX-2000 (9 mW/cm²) – A-CXL, 9*10] for the 40 keratoconic

corneas of 40 patients were described elsewhere (Bata et al. 2016). Patients were randomized to receive matrix therapy agent or placebo and the area of the corneal defect was measured in a dual manner, by conventional clinical methods (slit lamp biomicroscopy and fluorescein staining) and by UHR-OCT measurements. Serial corneal image data were acquired preoperatively and postoperatively every 48 hr until epithelial wound closure was achieved. A final visit where both tests were applied was performed 7–14 days after wound closure. Results of the wound area measurements have already been published (Bata et al. 2016). The current analysis evaluated the corneal wound healing in the 40 patients based on the three-dimensional data set for investigation of the epithelial thickness and the degree of reepithelization. In addition, it included the assessment of corneal microarchitectural changes.

Rabbit corneal wound healing model

The present analysis included 20 female New Zealand White rabbits (Charles River, Germany) from a randomized, masked, placebo-controlled study performed at the Department of Biomedical Research and the Center of Medical Physics and Biomedical Engineering at the Medical University of Vienna. The entire experiment was done in accordance with the Association for Research in Vision and Ophthalmology Statement for the Use of Animals in Ophthalmic and Vision Research and was approved by the local animal welfare committee. Details of the study design and animal handling are described elsewhere (Fischak et al. 2017). A central 6 mm diameter corneal scraping was induced using a trephine to delineate the wound. Epithelium (EP) was carefully removed with a dull-bladed knife to avoid damage of deeper corneal layers. Rabbits were randomized to receive either chitosan-*N*-acetylcysteine (C-NAC; Lacrimera[®], Croma Pharma GmbH, Leobendorf, Austria) or placebo. Tomographic imaging using UHR-OCT and photographic imaging of the cornea after fluorescein staining were performed to assess the baseline wound area and for documentation of the wound healing process at different time-points postinduction of the epithelial wound (24, 36, 48 and 72 hr). After the final measurement at 72 hr, while still under anaesthesia, animals were injected with Pentobarbital

(300 mg/kg of body weight) intravenously and euthanized. Cornea was immediately harvested and sent for pathological examination. Results of the wound area analysis have been published elsewhere (Fischak et al. 2017). The current analysis again evaluated the corneal wound healing based on the three-dimensional data set for investigation of epithelial thickness and degree of reepithelization. In addition, it included the assessment of microarchitectural changes in middle and deeper corneal layers.

Assessment of corneal wound healing

Ultrahigh-resolution OCT

Corneal wound healing in both species – humans and rabbits – was assessed using custom-built UHR-OCT machines operating in the 800 nm wavelength regime, differing primarily in the used light source technology. The system employed for imaging keratoconus patients used a Ti:Sapphire laser (Integral OCT; Femtolasers Produktions GmbH, Vienna, Austria) with a central wavelength of 800 nm. The full width at half maximum bandwidth of the source is 170 nm, which results in a theoretical axial resolution of approx. 1.2 μm in corneal tissue, when assuming group refractive indices for stroma and EP of 1.38 (Tuchin 2005) and 1.40 (Patel et al. 1995). The UHR-OCT for assessment of corneal wound healing in rabbits was based on a broad bandwidth superluminescent diode (Superlum cBLMD-T-850-HP-I; Superlum, Carrigtwohill, Cork, Ireland) operating at a central wavelength of 846 nm and providing a spectral bandwidth of 166 nm, which resulted in an axial resolution of 1.38 μm in tissue. The optical systems were designed in order to deliver optimal performance for the broad spectral bandwidth used for imaging and were described in detail elsewhere (Werkmeister et al. 2013; Aranha Dos Santos et al. 2015). The lateral resolution given by the parameters of the probe beam and the focal length of the scan lens objective used for focusing the probe beam onto the cornea were 20 and 21 μm for the human and the animal system, respectively. The maximum acquisition rate of both systems, given by the read out rate of the spectrometers CCD camera, was 70 kHz. The signal-to-noise ratio close to the zero delay was measured

with 97 dB (probe beam power of both systems set to 1.5 mW), and the sensitivity decay due to the finite spectrometer resolution was 10 dB to a depth of 1 mm. While data acquisition and visualization were done in Labview (Labview 2013; National Instruments, Austin, TX, USA), the postprocessing of spectral data was performed in MATLAB (MATLAB R2013b; The MathWorks Inc., Natick, MA, USA).

For *in vivo* measurements, the optical power of the probe beam incident on the subject's cornea was set to 1.5 mW for measurements on patients suffering from keratoconus and 2.5 mW for assessment of corneal wound healing in the animal model. Both values are well below the maximum permissible exposure of 8.6 mW for the current configuration, as specified by the safety standards (American National Standards Institute 2014; International Electrotechnical Commission 2014) to ensure ocular safety.

Head of the human subjects was stabilized on a modified slit lamp head rest; the patient was advised to fix an internal fixation target and to blink normally during the instrument alignment in front of the eye. Animals were placed in a custom-built holder allowing precise positioning of the animal with respect to the imaging system. Assessment of corneal wound healing in all experiments implied the acquisition of one OCT volume with a size of $7.5 \times 7.5 \times 1$ mm (horizontal \times vertical \times depth) and comprising $1024 \times 512 \times 1024$ voxels within a time interval of 5-seconds. Ultrahigh-resolution (UHR) OCT images were yielded after postprocessing of the spectral data, and motion artefacts in between acquired images caused by involuntary eye movements of the subject were compensated based on cross-correlation of consecutive images (Thevenaz et al. 1998). Thereafter, the corneal EP was segmented in the cross-sectional images in an automatic manner. After correction for the incidence angle of the probe beam and corneal curvature, assuming an anterior corneal radius of 7.8 mm (Gullstrand 1924) and 8.4 mm (Zhang et al. 2017) in the human and the rabbit eye, respectively, epithelial thickness maps were created. The maps allowed for precise quantification of the wound area, central epithelial thickness (CET) and time-course of wound closure. In keratoconus patients,

the depth of the stromal demarcation line (DL) after accelerated epi-off CXL was evaluated, using the central OCT scan of the horizontal meridian at five positions on the cornea (centrally, 1.2 and 2.4 mm temporally, 1.2 and 2.4 mm nasally). The front surface of the corneal EP was used as tomographic landmark for thickness measurements.

Fluorescein staining

In all experiments, clinical assessment of the corneal wound was based on instilling one drop of Fluorescein (Minims-Fluorescein Sodium 2.0%; Chauvin Pharmaceuticals Ltd., London, UK) into the study eye. Images of the healing process were obtained by photographic technology. In humans, a digital camera captured the corneal defect, while the patient was examined with a cobalt-blue light attached to a standard biomicroscope (BQ 900; Haag Streit AG, Koeniz, Switzerland). In rabbit's cornea, digital photographs were taken by means of a custom-built set-up, under illumination with a cobalt-blue light filter.

To investigate the corneal wound healing process in both species, the surface area of the corneal defect was semi-automatically measured by a custom written IMAGEJ software (National Institutes of Health, available in the public domain at <https://rsbweb.nih.gov/ij/>); segmentation of the stained area was based on the analysis of the image histogram. In keratoconus patients, the iris was detected by application of an edge filter to the fluorescein photography and its area was calculated. The wound healing process was then evaluated by calculating the time-course of the wound-to-iris-ratio.

For assessment of the wound area in the animal model, a ruler was placed in the same focal plane close to the eye while corneal photography was acquired. This allowed accurate calculations of image dimensions and wound size.

Statistical analysis

A paired *t*-test was performed to compare the CET at baseline versus final visit, while a one-way ANOVA model for repeated measurements was employed to test differences between the treatment groups. Continuous variables are given as means \pm standard deviation (SD). A *p*-value <0.05 was considered the level of significance.

Statistical analysis was performed using SPSS version 24 (SPSS; IBM, Armonk, NY, USA).

Results

Patients with keratoconus

Figure 1 illustrates UHR-OCT tomograms of a keratoconus patient at the baseline visit and 4 days after epi-off CXL treatment. All layers of the human cornea, including EP, basal layer of the EP (BLE), BL, corneal stroma (ST), Descemet's membrane (DM) and the endothelium (ED) were visualized. In addition, the precorneal tear film could be seen as the top-most reflective band at the corneal surface. The cross-sectional image through the horizontal meridian in Fig. 1A revealed the typical thinning of the EP in the inferotemporal zone (green arrow) and a compensatory thickening in the opposite superonasal zone of the cornea, before treatment. At 4 days after treatment, despite complete wound closure that could be clinically documented by negative fluorescein staining, UHR-OCT in Fig. 1B revealed small irregularities in the central and paracentral epithelial surface, indicative for a still ongoing healing process or contact lens wear. The thinnest and the thickest EP were located at 2.5 mm inferiorly and 1 mm superiorly from the corneal vertex. Gross evaluation of the epithelial thickness in the tomograms below indicated a thinner 'new' epithelial layer 4 days after accelerated epi-off CXL.

Three-dimensional epithelial thickness maps extracted from the UHR-OCT data during corneal healing in treated keratoconus patients are shown in Fig. 2B before and Fig. 2C–F after epi-off CXL. The thinnest region of the EP, as evaluated from the map in Fig. 2B, was found in the inferotemporal part of the cornea and corresponded well with the steepest corneal region as extracted by Scheimpflug tomography as depicted in Fig. 2A.

Figure 2C clearly illustrates the presence of an epithelial erosion 2 days after CXL in the centre of the map with the full thickness epithelial defect, reaching BL; as such, no epithelial (zero) thickness was measured at some locations. Cross-sectional images of the same patient and the same time point (2 days after CXL) are shown in Fig. 3. The tomograms obtained at different

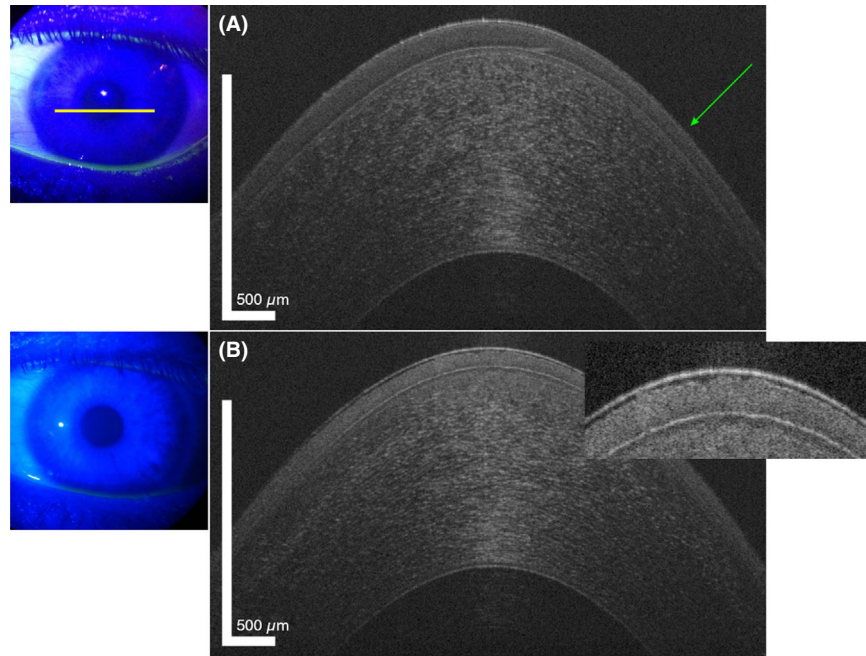


Fig. 1. Ultrahigh-resolution (UHR)-optical coherence tomography (OCT) cross-sectional images on the horizontal meridian of the paracentral cornea in a patient with progressive keratoconus. Imaging at (A) the baseline visit revealed epithelial thinning in the inferotemporal cornea. (B) Four days after crosslinking procedure, despite apparently clinical complete epithelial closure, UHR-OCT revealed multiple irregularities in the epithelial surface, indicating incomplete epithelial healing.

locations of the cornea revealed different degrees of reepithelization, with deep defects still reaching BL in the inferior part of the wound. Epithelial cells were identified as already consolidating their attachment to the underlying basement membrane in the mid and superior part. Imaging with UHR-OCT identified these precise details of corneal wound healing, while clinical evaluation via fluorescein staining and slit lamp examination, as illustrated by Fig. 3A could only reveal the borders of the wound, but did not provide any information about its depth or the progress of epithelial regrowth. The thickness maps obtained in this keratoconus patient proved to be an accurate instrument for monitoring the reepithelization process and indicated complete wound closure 4 days after CXL treatment, with a thinner EP as compared to baseline. The same finding was present 15 days after surgery, when the measured epithelial thickness was $35.9 \mu\text{m}$, significantly lower than the baseline value of the same patient ($56.6 \mu\text{m}$).

Epithelial thickness measurements performed in all 40 eyes over an area of $4 \text{ mm} \times 4 \text{ mm}$ around the corneal apex yielded $43.8 \pm 6.37 \mu\text{m}$ at baseline versus $35.0 \pm 5.8 \mu\text{m}$ at the last visit, which

was significantly thinner after reepithelization ($p < 0.001$). No statistically significant difference was found between the treatment groups ($p = 0.61$). The mean central corneal thickness (CCT) in all patients before the CXL procedure was $482.7 \pm 38.2 \mu\text{m}$. Surgical success in the treated keratoconus patients was assessed by identification of the stromal DL and measurement of its central depth (absolute values and depth percentage in respect to the entire corneal thickness). Using UHR-OCT data, DL was identified at $43.7 \pm 13.5\%$ stromal depth, after a mean of 20 ± 5 days post-CXL procedure. Absolute values for the stromal depth of the DL were as follows: $190.2 \pm 54.6 \mu\text{m}$ (2.4 mm temporal), $195.4 \pm 58.9 \mu\text{m}$ (1.2 mm temporal), $211.1 \pm 63.2 \mu\text{m}$ (central), $206.5 \pm 67.0 \mu\text{m}$ (1.2 mm nasal) and $204.2 \pm 52.6 \mu\text{m}$ (2.4 mm nasal). Figure 4 illustrates an UHR cross-sectional image of a patient 15 days after CXL, where the DL was clearly visible.

Rabbit corneal wound healing model

A different epithelial healing process was studied in rabbit cornea. Figure 5 shows a comparison between an UHR cross-sectional image of the paracentral

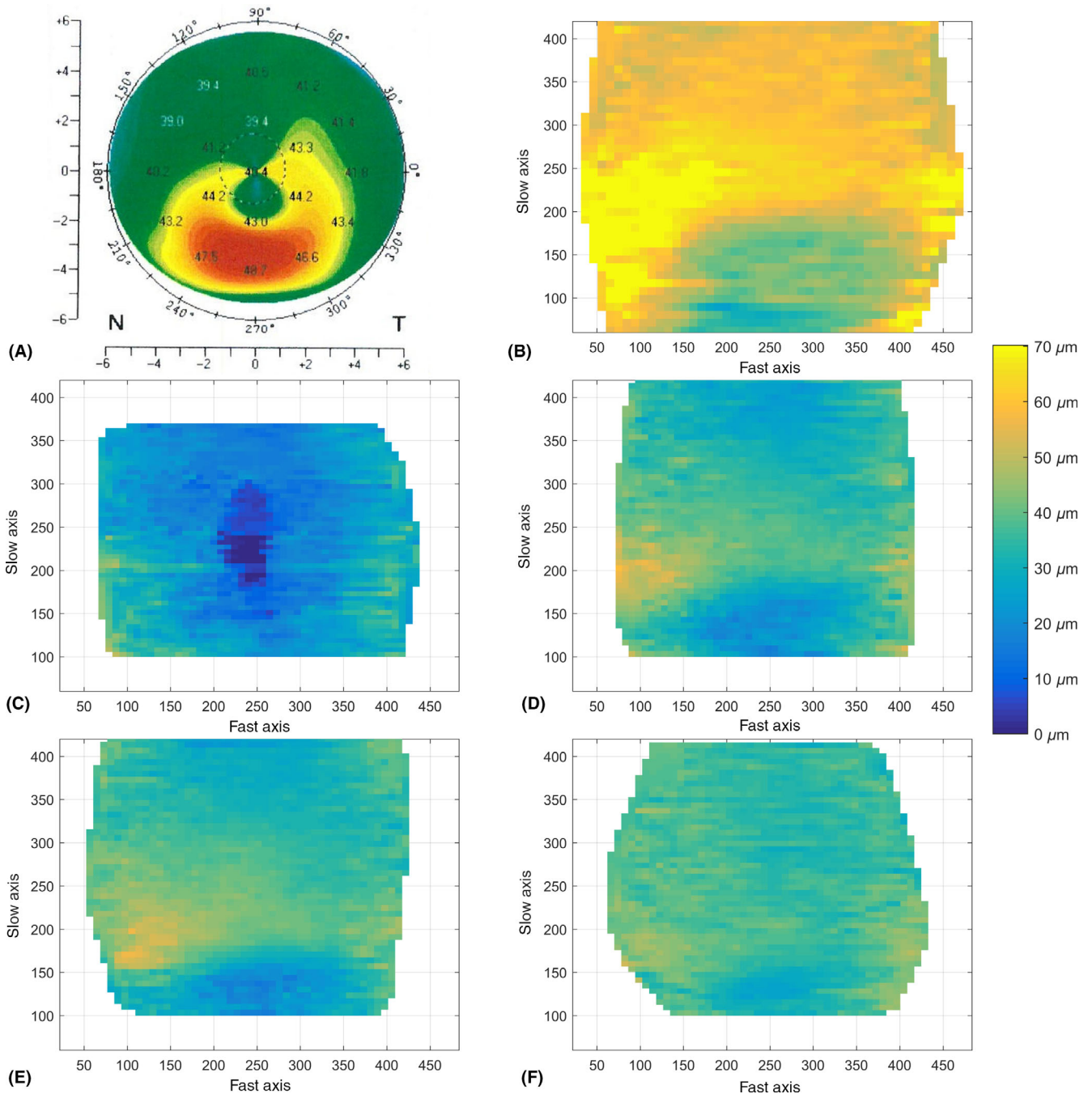


Fig. 2. Corneal imaging of a keratoconus patient before and after an accelerated epi-off crosslinking (CXL) procedure. Corneal topography by (A) Scheimpflug tomography revealing the steepest corneal region in the inferotemporal part corresponding well with the thinnest zone of the epithelium as extracted from (B) ultrahigh-resolution-optical coherence tomography data sets. Epithelial thickness maps correspond to measurements performed (B) preoperatively, at baseline and during corneal healing after treatment at different time-points (C) 2 days, (D) 4 days, (E) 6 days and (F) 15 days after CXL.

cornea of a New Zealand White rabbit and a histology specimen stained with Hematoxylin & Eosin (H&E, 10× magnification). The resolution of the system was sufficient to resolve, comparable to histology, all corneal layers, including EP, ST, DM and corneal ED. Furthermore, given by the cell shape and their hyporeflective appearance,

the BLE can be distinguished as a band within the EP showing lower reflectivity (Werkmeister et al. 2017). It is unclear from both literature and image data if there is a ‘true’ BL in rabbits that separates EP from stroma. If identified, it is described as a structure with a thickness of 1–3 μm (Hayashi et al. 2002; Gwon 2008) considered to

represent a modified zone of the anterior stroma (Gwon 2008). This thickness is much smaller than in the human corneas, where using a similar UHR-OCT – an average thickness in the range of 18 μm (Werkmeister et al. 2017) was found. In the UHR scan depicted in Fig. 5B, BL appeared as a regular band underlying the EP.

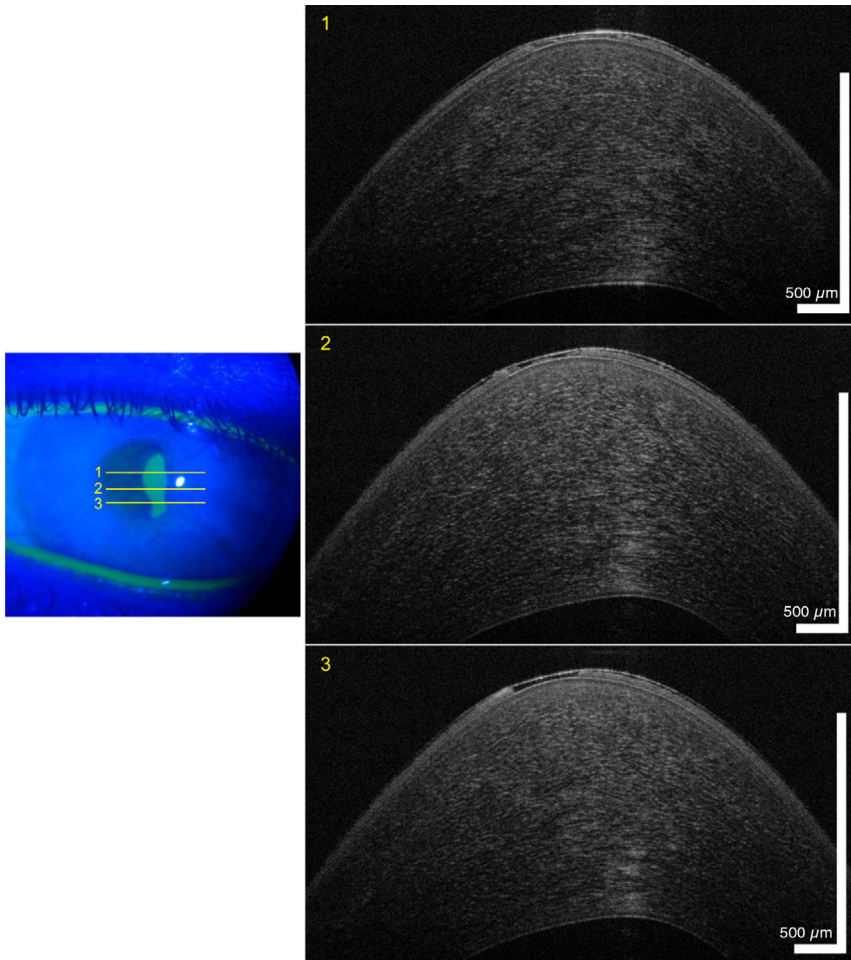


Fig. 3. Corneal epithelial wound in a keratoconus patient after epi-off crosslinking. Fluorescein staining and anterior segment biomicroscopy (diffuse illumination with cobalt-blue filter) illustrate the defect, as seen by clinical methods. Corresponding ultrahigh-resolution-optical coherence tomography images acquired 2 days after surgical intervention at three different locations revealing different degrees of reepithelialization.

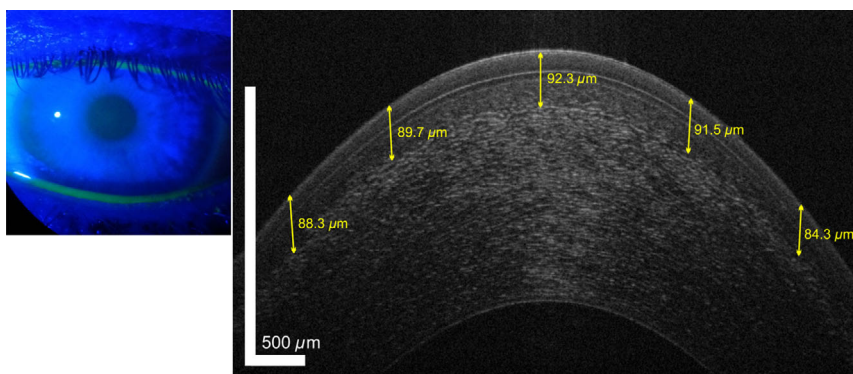


Fig. 4. Ultrahigh-resolution cross-sectional image of a patient 15 days after crosslinking revealing the stromal depth of the demarcation line. Graphical landmarks take the incidence angle of the probe beam and its refraction at the air-tear interface into account.

Significantly thinner than the CCT in healthy humans, the CCT in rabbits at baseline was found to be $303.1 \pm 18.6 \mu\text{m}$, comparable to histological data (Gwon 2008). In Fig. 6, an

exemplary cross-sectional image of a corneal wound 24 hr after iatrogenic corneal injury is depicted. Figure 6A using Fluorescein staining clearly revealed the corneal defect as seen by

slit lamp examination. In the UHR-OCT in Fig. 6B, the epithelial erosion with the wound depth reaching BL could be observed. In addition, corneal oedema after epithelial scraping was visualized. Over the study period of 72 hr, oedema subsided to nearly the original corneal thickness while corneal healing occurred (ref. Fig. 8). Furthermore, in all 20 eyes an average thickening of the central ED from $4.4 \pm 0.8 \mu\text{m}$ at baseline to $5.3 \pm 0.9 \mu\text{m}$ 72 hr after setting of the wound was observed ($p = 0.004$).

Three-dimensional UHR-OCT data were used for creation of epithelial thickness maps showing the time-course of CET measurements and wound closure over the study period of 72 hr (Fig. 7).

In the measurements depicted in Fig. 7, initial epithelial thickness at baseline was $34.9 \mu\text{m}$. The maps in Fig. 7B–D illustrate the depth of the corneal wound reaching BL; during epithelial healing gradual reduction of the defect areas was recorded, as following: 8.2 , 5.5 and 3.4 mm^2 at different time-points 24, 36 and 48 hr after wound creation. Furthermore, in Fig. 7C,D a thickening of the EP at the wound margins can be observed. In the exemplary case, 72 hr after surgery, complete wound closure and reepithelialization with a CET of $33.2 \mu\text{m}$ were shown. Based on UHR-OCT data, average CET in all rabbits at the beginning of the study period was measured as $35.9 \pm 2.6 \mu\text{m}$. In the ten rabbits that revealed complete wound closure after 72 hr, CET at this time point was significantly smaller than at baseline ($30.4 \pm 2.8 \mu\text{m}$ versus $35.4 \pm 2.9 \mu\text{m}$, $p = 0.005$).

In Fig. 8, an UHR-OCT scan of a rabbit receiving topical C-NAC obtained 72 hr after inducing the epithelial defect is shown. While healing, anterior ST exhibited changes in optical scattering and absorption properties within the stroma, which appeared very similar to the DL observed after CXL in humans. The depth of inner-stromal reflectivity alteration was assessed in all rabbits at 72 hr after inducing the corneal wound. Ultrahigh-resolution (UHR) OCT measurements on the horizontal meridian assessed the DL-like structure at $66.6 \pm 16.1 \mu\text{m}$ (2.4 mm temporal), $84.6 \pm 16.9 \mu\text{m}$ (1.2 mm temporal), $90.7 \pm 18.7 \mu\text{m}$ (central), $87.8 \pm 14.3 \mu\text{m}$ (1.2 mm nasal) and $78.5 \pm 11.9 \mu\text{m}$ (2.4 mm nasal) or

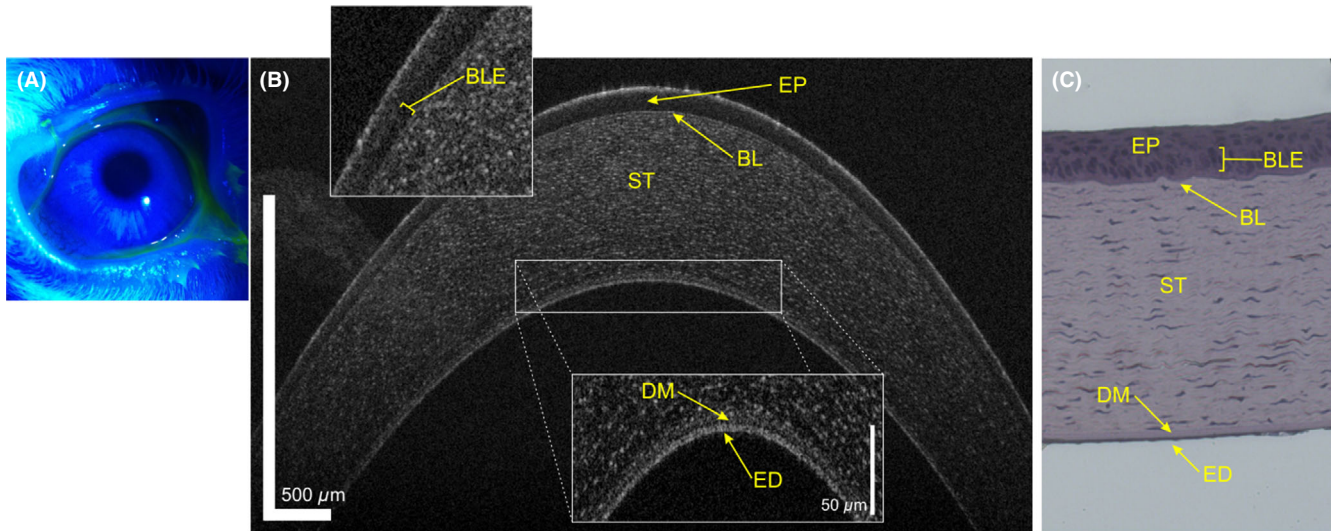


Fig. 5. Imaging of the central cornea of a New Zealand White rabbit by (A) slit lamp photography, (B) UHR-OCT and (C) histology specimen with H&E staining (10×magnification). Non-invasive *in vivo* imaging via UHR-OCT visualizes all corneal layers as seen histology: BL = Bowman's layer, BLE = basal layer of EP, DM = Descemet's membrane, ED = endothelium, EP = epithelium, ST = corneal stroma.

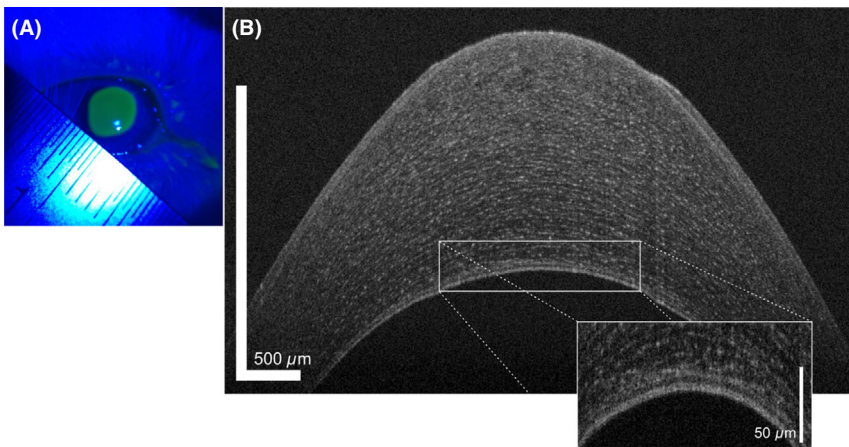


Fig. 6. Iatrogenic corneal wound in a Zealand White rabbit visualized via (A) slit lamp photography and (B) UHR-OCT imaging. Twenty-four hrs after corneal iatrogenic trauma, a complete epithelial defect reaching the corneal stroma is revealed; posttraumatic corneal oedema and a thickening of the endothelium are also identified in this case.

30.0 ± 5.1% stromal depth. This morphological feature could not be identified in the histological specimen, given in Fig. 8B.

Comparison of the histological specimen obtained from eyes treated with C-NAC versus placebo revealed a less organized EP with fewer cells in the superficial epithelial layers and larger intercellular spaces in the placebo group. In addition, diffuse corneal oedema caused disturbances in parallel arrangement of the collagen lamellae. Furthermore, few fixation artefacts could be observed but did not influence the interpretation of the architectural change.

Discussion

Optical coherence tomography (OCT) technology allows precise investigations of ocular structures in a non-invasive, non-contact and cross-sectional manner. Recent developments in UHR-OCT (Werkmeister et al. 2017) provide imaging instruments capable of offering insight to fine anatomical landmarks and their quantitative assessment.

Our study tried to demonstrate the unique capability of a custom-built UHR-OCT machine to identify the dynamic changes in the corneal EP during early corneal wound healing phases in two different species.

In current clinical practice, the assessment of any corneal lesion is mainly performed by fluorescein staining and direct measurement of the corneal defect during AS biomicroscopy (slit lamp examination). Photographic systems attached to the slit lamp facilitate acquisition of two-dimensional images of the corneal wounds. Generally, sodium fluorescein staining occurs by three mechanisms (Mokhtarzadeh et al. 2011): pooling, ingress around the cells and inside the cells in case of cellular apoptosis. By examination, only the pooling effect can be assessed. This method, however, is limited, since the measurement of wound size itself becomes challenging, given by the fact that it is dependent on complex optical properties such as the distance to the measured eye, refractive error of the examiner, and the magnification of the imaging device (Fischak et al. 2017). To overcome these inconveniences, authors have initially calibrated the photographs of the ocular surface, and, thereafter calculated the area of the epithelial defect (Fischak et al. 2017). The same lesions were also assessed with the UHR-OCT system, for comparing and contrasting reasons.

In Fig. 1A, a cross-sectional image through the horizontal meridian of a keratoconic cornea showed initial epithelial changes, that is, a thinned area in the paracentral cornea, while in the opposite part, a compensatory thickening of the EP was noted before treatment. The exact location of the thinned

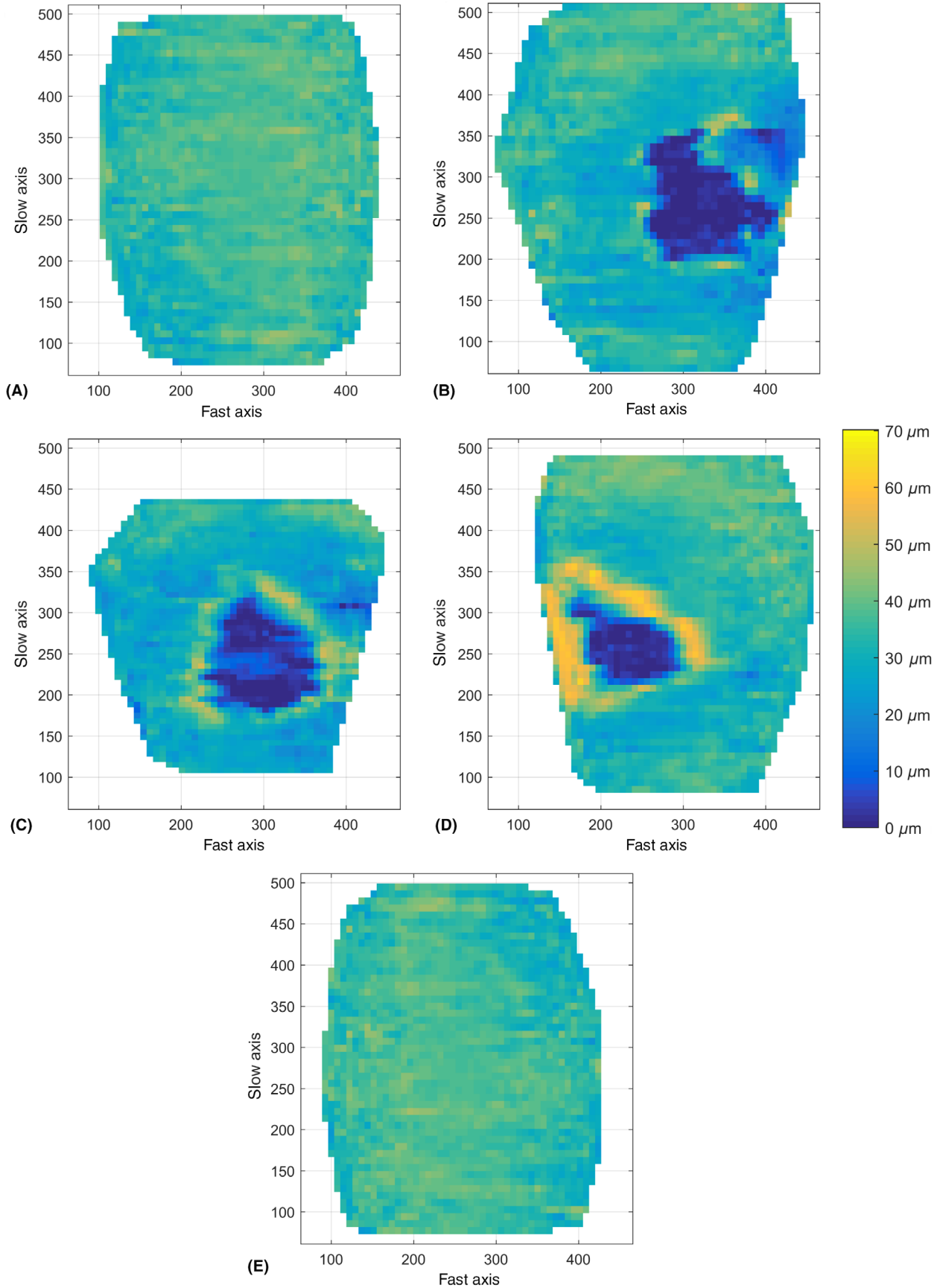


Fig. 7. Epithelial thickness maps in a rabbit wound healing model reconstructed from ultrahigh-resolution-optical coherence tomography data. The maps refer to measurements at (A) baseline and later time-points (B) 24 hr, (C) 36 hr, (D) 48 hr and (E) 72 hr after experimental creation of a corneal wound.

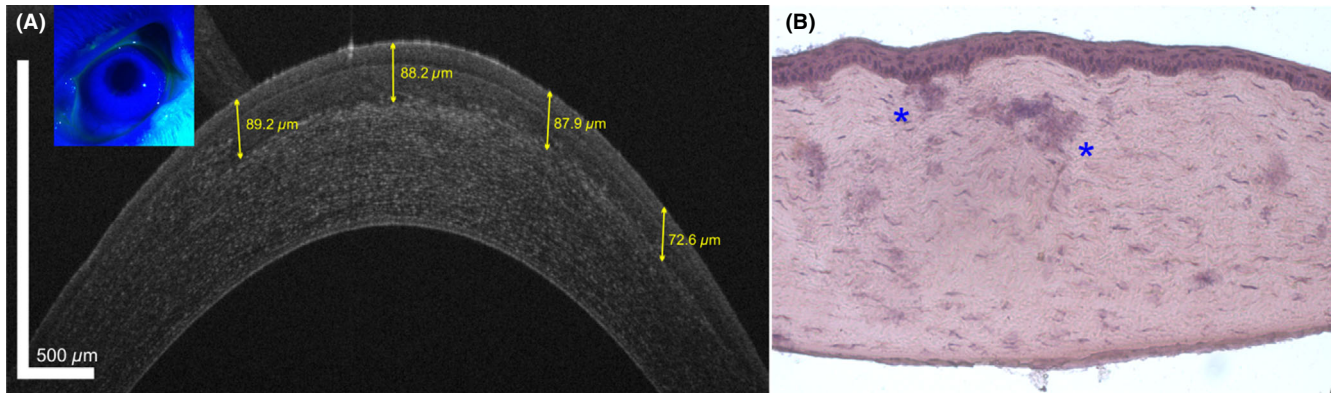


Fig. 8. Imaging of a New Zealand White rabbit treated with C-NAC (Lacrimera[®]) 72 hr after iatrogenic corneal injury. The ultrahigh-resolution-optical coherence tomography (OCT) cross-sectional image in (A) shows alterations in the scattering properties within the anterior stroma, similar to a demarcation line (DL) in humans after crosslinking keratoconus treatment. Graphical landmarks take the incidence angle of the OCT probe beam and its refraction at the air-tear interface into account. (B) The histological image with H&E staining of the same cornea revealed diffuse oedema but no distinct DL-like landmark could be identified. The blue asterisks in (B) indicate fixation artefacts during specimen preparation.

epithelial area corresponded well with the steepest corneal region detected by Scheimpflug tomography, as previously described by Werkmeister et al. (2017).

Four days after treatment, wound healing was apparently completed when assessed by clinical examination and negative fluorescein staining. In contrast, UHR-OCT in Fig. 1B depicts significant epithelial irregularities at the corneal apex after accelerated epi-off CXL.

The tear film has the same 'compensatory' properties for small irregularities on the front corneal surface as the EP does for the minor stromal irregularities. Conventional AS-OCT systems are not capable of resolving the border between tear film and EP, thus epithelial thickness might be overestimated by the thickness of the tear film adding 2–8 μm in value (Azartash et al. 2011) and minor irregularities in the epithelial surface can be masked by the overlying tear film. Therefore, the exact quantification of the epithelial thickness and morphology could be modified if the tear film is included in the measurements (Reinstein et al. 2015). Based on previously published data (Werkmeister et al. 2013, 2017; Aranha Dos Santos et al. 2015), the UHR-OCT employed for the current study is capable of measuring both tear film thickness and epithelial thickness with high accuracy, thus, evaporation and movement of the tear film did not cause any artefacts in our measurements. Epithelial thickness maps extracted from the OCT data were obtained after corrections of both

corneal curvature and incident angle of the probe beam (Werkmeister et al. 2017). The analysis of the epithelial thickness map in keratoconus patients before CXL indicated a significant epithelial remodelling (inferior thinning versus superior thickening). After treatment, complete epithelial healing was documented by the thickness maps. Furthermore, at the time point of the final visit, the new epithelial layer was found to be thinner than before treatment. Hence, epithelial mapping via UHR-OCT could be applied to gain insight upon corneal healing process after CXL, both on short term, as in our study, and on longer term. As shown before, based on the epithelial thickness maps, certain parameters have gained early diagnostic properties in keratoconus (Li et al. 2012). Moreover, the epithelial thickness profile appears to be more sensitive than corneal topography in this respect (Kanellopoulos et al. 2012).

In Fig. 3, the clinical evaluation identified the borders of the corneal defect by indirect visualization, as fluorescein stained only the area where EP was absent. UHR-OCT detected exactly the margins of the epithelial defect, based on different reflectivity of the different corneal layers and on providing additional information about the depth of the according reflector. The cross-sectional scans at different levels through the wound proved that at the apex of the cornea the wound internal architecture and depth were highly variable depending

on the scanned location. Irregularities in the corneal EP were visible, indicating ongoing healing, as EP started to form new layers by attaching themselves to the basal membrane support.

Additional corneal healing information could be gained also from the tomogram in Fig. 4. Crosslinking (CXL) acts unevenly within the corneal thickness (Spadea et al. 2016) as proven by the different depths where the DL was identified (central versus paracentral, temporal versus nasal). The procedure causes a dose dependent keratocyte damage (Spadea et al. 2016). By using the slit lamp, the DL becomes visible as early as 2 weeks (Spadea et al. 2016) and defines the transition zone from the cross-linked cornea and non-cross-linked cornea. It can be identified as an area of increased reflectivity due to different refractive indexes between the two corneal regions, but no accurate depth can be measured in a clinical setting. Doors et al. (2009) described the best visibility of DL by AS-OCT at 1 month post-CXL treatment, with an average depth of 313 μm . The keratoconus patients from our study underwent an accelerated procedure; therefore, the depth of the DL is shallower than in the standard protocols (Pircher et al. 2018). In our study, UHR-OCT provided good visualization of the DL earlier than 3 weeks after CXL, as shown in Fig. 4.

In the rabbit cornea, UHR-OCT provided near histological details (Fig. 5); same anatomical landmarks as in humans, that is, EP, BL, stroma,

Descemet membrane and ED were identified. The rabbit cornea was chosen as animal model based on similarities in anatomy and in the wound healing mechanisms as compared to the human cornea (Torricelli et al. 2013). In analogy to the measurements in humans, UHR-OCT was employed for assessment of the epithelial defect in rabbit cornea and comparison with photographic data after fluorescein staining. Ultrahigh-resolution (UHR) OCT data allowed for clear identification of the wound margins, wound depth and degree of reepithelization. This facilitated a more objective evaluation of the wound healing as compared to a slit lamp examination. Additionally, the OCT data revealed some subtle changes in deeper layers of the cornea that could not be identified using biomicroscopy. Here, UHR-OCT visualized a thickening of the ED in the range of 1 μm during the early corneal healing phase <24 hr after epithelial injury. This could be explained by the overall changes occurring in the cornea after trauma, when mitotic activity of the ED increases after the first 24 hr (Gwon 2008). Usually, these changes intensify around the wound area during the subsequent 48–55 hr, particularly in endothelial or posterior stromal wounds (Gwon 2008). Yet, our data point out that even in superficial corneal wounds there are visible changes in the entire corneal structure, including ED (Fig. 6). The average endothelial thickness measured *in vivo* in rabbits using UHR-OCT corresponded well with values of 3–5 μm provided by the literature and yielded from histological examinations (Gwon 2008).

Epithelial thickness maps in rabbits revealed the healing dynamics within the first 72 hr after corneal wound induction (Fig. 7). After complete epithelization, thickness of the renewed tissue was lower than the baseline measurements, proving ongoing changes until finalization of corneal healing process beyond wound closure. Moreover, as depicted in Fig. 8, using UHR-OCT we were able to identify a feature of corneal healing in rabbit cornea at 72 hr after creation of the wound. A structure similar to the DL was detected in the central area beneath the initial epithelial defect. Several mechanisms for the appearance of such anatomical landmarks are

known. Epithelial abrasions trigger changes in the anterior stroma related to keratocyte apoptosis (Helena et al. 1998). One event is elicited by the direct mechanical trauma, the other is determined by inflammatory cytokines recruited during epithelial injury (McGrath & Lee 2013). Such ‘cross-talking’ mechanisms borrowed from the stromal healing (Ljubimov & Saghizadeh 2015) could explain the change in reflectivity that was detected. The mechanism is similar to CXL, however not initiated photo-chemically but mechanically giving the same appearance in the OCT cross-sectional images. The DL-like structural change as landmark was not identifiable in histology, since its formation is related to changes in the refractive index within the stroma as a result of an increase in collagen fibre diameter and fibril spacing. Therefore, when histology specimens are prepared and dyes are impregnated into the tissue, the colouration remains homogenous within the corneal depth and no DL becomes visible (Dahl et al. 2012).

Corneal healing includes two successive phases: latent (lag) and final (closure), respectively. The initial phase includes cellular and subcellular remodelling at the margins of the defect, whereas the wound closure is based on the restoration of the multicellular architecture of the EP (Ljubimov & Saghizadeh 2015). Both phases could be identified using UHR-OCT, in a non-invasive, fast manner, without the inconveniences of pathology specimen, where corneal landmarks and measurements might be biased by fixation artefacts.

In conclusion, the results of our study proved the capability of a custom-built UHR-OCT system to assess the fine details of corneal microarchitectural changes induced by the healing after superficial epithelial trauma – iatrogenic or surgical – in two different species. Monitoring of corneal wound healing by UHR-OCT offers a great advantage over the conventional clinical assessment including slit lamp examination and fluorescein staining by an increased accuracy, objectiveness and capability for three-dimensional mapping of the defect. In addition, morphological changes in the tissue both in proximity of the wound and in deeper corneal layers that are occurring during the epithelial

healing process could be revealed. With these, it might provide a deeper insight into corneal regeneration mechanisms and facilitate future investigations of wound healing therapies and their efficacy.

References

- American National Standards Institute (2014): American national standard for safe use of lasers. Orlando, FL: The Laser Institute of America; 2000. ANSI Z136.1-2014.
- Aranha Dos Santos V, Schmetterer L, Groschl M et al. (2015): *In vivo* tear film thickness measurement and tear film dynamics visualization using spectral domain optical coherence tomography. *Opt Express* **23**: 21043–21063.
- Azartash K, Kwan J, Paugh JR, Nguyen AL, Jester JV & Gratton E (2011): Pre-corneal tear film thickness in humans measured with a novel technique. *Mol Vis* **17**: 756–767.
- Bata AM, Witkowska KJ, Wozniak PA et al. (2016): Effect of a matrix therapy agent on corneal epithelial healing after standard collagen cross-linking in patients with keratoconus: a randomized clinical trial. *JAMA Ophthalmol* **134**: 1169–1176.
- Dahl BJ, Spotts E & Truong JQ (2012): Corneal collagen cross-linking: an introduction and literature review. *Optometry* **83**: 33–42.
- Doors M, Tahzib NG, Eggink FA, Berendschot TT, Webers CA & Nuijts RM (2009): Use of anterior segment optical coherence tomography to study corneal changes after collagen cross-linking. *Am J Ophthalmol* **148**: 844–851.e842.
- Fischak C, Klaus R, Werkmeister RM, Hohe-nadl C, Prinz M, Schmetterer L & Garhofer G (2017): Effect of topically administered chitosan-N-acetylcysteine on corneal wound healing in a rabbit model. *J Ophthalmol* **2017**: 5192924.
- Gora M, Karnowski K, Szkulmowski M, Kaluzny BJ, Huber R, Kowalczyk A & Wojtkowski M (2009): Ultra high-speed swept source OCT imaging of the anterior segment of human eye at 200 kHz with adjustable imaging range. *Opt Express* **17**: 14880–14894.
- Grieve K, Paques M, Dubois A, Sahel J, Boccara C & Le Gargasson JF (2004): Ocular tissue imaging using ultrahigh-resolution, full-field optical coherence tomography. *Invest Ophthalmol Vis Sci* **45**: 4126–4131.
- Gullstrand A (1924): The dioptries of the eye. In: Southall J (ed.). *Helmholtz's treatise on physiological optics*. Rochester, NY: Optical Society of America 382–415.
- Guthoff RF, Zhivov A & Stachs O (2009): *In vivo* confocal microscopy, an inner vision of the cornea - a major review. *Clin Exp Ophthalmol* **37**: 100–117.
- Gwon A (2008): The rabbit in cataract/IOL surgery. In: Tsonis PA (ed.). *Animal models*

- in eye research. San Diego, CA: Elsevier 184–199.
- Hayashi S, Osawa T & Tohyama K (2002): Comparative observations on corneas, with special reference to Bowman's layer and Descemet's membrane in mammals and amphibians. *J Morphol* **254**: 247–258.
- Helena MC, Baerveldt F, Kim WJ & Wilson SE (1998): Keratocyte apoptosis after corneal surgery. *Invest Ophthalmol Vis Sci* **39**: 276–283.
- International Electrotechnical Commission (2014): International Electrotechnical Commission IEC 60825-1, Safety of laser products - Part 1: Equipment classification and requirements (IEC 60825-3:2014). Available at XXXXX. (Accessed on DD MM YYYY).
- Kanellopoulos AJ, Aslanides IM & Asimellis G (2012): Correlation between epithelial thickness in normal corneas, untreated ectatic corneas, and ectatic corneas previously treated with CXL; is overall epithelial thickness a very early ectasia prognostic factor? *Clin Ophthalmol* **6**: 789–800.
- Lagali N, Germundsson J & Fagerholm P (2009): The role of Bowman's layer in corneal regeneration after phototherapeutic keratectomy: a prospective study using *in vivo* confocal microscopy. *Invest Ophthalmol Vis Sci* **50**: 4192–4198.
- Li Y, Tan O, Brass R, Weiss JL & Huang D (2012): Corneal epithelial thickness mapping by Fourier-domain optical coherence tomography in normal and keratoconic eyes. *Ophthalmology* **119**: 2425–2433.
- Liu CY & Kao WW (2015): Corneal epithelial wound healing. *Prog Mol Biol Transl Sci* **134**: 61–71.
- Ljubimov AV & Saghizadeh M (2015): Progress in corneal wound healing. *Prog Retin Eye Res* **49**: 17–45.
- Luo J, Yao PJ, Li MY, Xu GC, Zhao J, Tian M & Zhou XT (2015): Quantitative analysis of microdistortions in Bowman's layer using optical coherence tomography after SMILE among different myopic corrections. *J Refract Surg* **31**: 104–109.
- McGrath LA & Lee GA (2013): Corneal debridement update: adjuvant therapies and wound healing. *Asia Pac J Ophthalmol (Phila)* **2**: 237–243.
- Mokhtarzadeh M, Casey R & Glasgow BJ (2011): Fluorescein punctate staining traced to superficial corneal epithelial cells by impression cytology and confocal microscopy. *Invest Ophthalmol Vis Sci* **52**: 2127–2135.
- Patel S, Marshall J & Fitzke FW 3rd (1995): Refractive index of the human corneal epithelium and stroma. *J Refract Surg* **11**: 100–105.
- Pircher N, Lammer J, Holzer S, Gschliesser A, Donner R, Peh S & Schmidinger G (2018): Correlation between central stromal demarcation line depth and changes in K values after corneal cross-linking (CXL). *Graefes Arch Clin Exp Ophthalmol* **256**: 759–764.
- Reinstein DZ, Dickeson Z, Archer TJ & Gobbe M (2014): Artemis very high frequency digital ultrasound-guided femtosecond laser recut after flap complication. *Digit J Ophthalmol* **20**: 43–57.
- Reinstein DZ, Yap TE, Archer TJ, Gobbe M & Silverman RH (2015): Comparison of corneal epithelial thickness measurement between Fourier-domain OCT and very high-frequency digital ultrasound. *J Refract Surg* **31**: 438–445.
- Rocha KM, Perez-Straziota CE, Stulting RD & Randleman JB (2014): Epithelial and stromal remodeling after corneal collagen cross-linking evaluated by spectral-domain OCT. *J Refract Surg* **30**: 122–127.
- Schmoll T, Unterhuber A, Kolbitsch C, Le T, Stingl A & Leitgeb R (2012): Precise thickness measurements of Bowman's layer, epithelium, and tear film. *Optom Vis Sci* **89**: E795–E802.
- Shroff R, Francis M, Pahuja N, Veeboy L, Shetty R & Roy AS (2016): Quantitative evaluation of microdistortions in Bowman's layer and corneal deformation after small incision lenticule extraction. *Transl Vis Sci Technol* **5**: 12.
- Spadea L, Tonti E & Vingolo EM (2016): Corneal stromal demarcation line after collagen cross-linking in corneal ectatic diseases: a review of the literature. *Clin Ophthalmol* **10**: 1803–1810.
- Thevenaz P, Ruttimann UE & Unser M (1998): A pyramid approach to subpixel registration based on intensity. *IEEE Trans Image Process* **7**: 27–41.
- Toricelli AA, Singh V, Santhiago MR & Wilson SE (2013): The corneal epithelial basement membrane: structure, function, and disease. *Invest Ophthalmol Vis Sci* **54**: 6390–6400.
- Tuchin VV (2005): Optical clearing of tissue and blood. Bellingham, WA: SPIE Publications.
- Werkmeister RM, Alex A, Kaya S et al. (2013): Measurement of tear film thickness using ultrahigh-resolution optical coherence tomography. *Invest Ophthalmol Vis Sci* **54**: 5578–5583.
- Werkmeister RM, Sapeta S, Schmidl D et al. (2017): Ultrahigh-resolution OCT imaging of the human cornea. *Biomed Opt Express* **8**: 1221–1239.
- World Medical Association (2013): World Medical Association Declaration of Helsinki: ethical principles for medical research involving human subjects. *JAMA* **310**: 2191–2194.
- Yasuno Y, Madjarova VD, Makita S et al. (2005): Three-dimensional and high-speed swept-source optical coherence tomography for *in vivo* investigation of human anterior eye segments. *Opt Express* **13**: 10652–10664.
- Zhang H, Qin X, Cao X, Zhang D & Li L (2017): Age-related variations of rabbit corneal geometrical and clinical biomechanical parameters. *Biomed Res Int* **2017**: 3684971.
- Zhou W & Stojanovic A (2014): Comparison of corneal epithelial and stromal thickness distributions between eyes with keratoconus and healthy eyes with corneal astigmatism ≥ 2.0 D. *PLoS ONE* **9**: e85994.

Received on October 2nd, 2018.
Accepted on January 19th, 2019.

Correspondence:

René M. Werkmeister
Center for Medical Physics and Biomedical Engineering
Medical University of Vienna
Währinger Gürtel 18-20, 4L
1090 Vienna
Austria
Tel: +43 1 40400 19940
Fax: +43 1 40400 39880
Email: rene.werkmeister@meduniwien.ac.at

The financial support by the Christian Doppler Research Association, the Austrian Federal Ministry of Digital and Economic Affairs and the National Foundation of Research, Technology and Development as well as the Hochschuljubiläumstiftung der Stadt Wien (project H-289408/2013) is gratefully acknowledged. Thea Pharma provided the study drugs for the clinical trial in humans. Croma-Pharma provided test substances evaluated within the rabbit cornea wound healing model. This project was funded by the Christian Doppler laboratory for 'Ocular and dermal effects of Thiomers'.